ORIGINAL ARTICLE

Added value of quantitative parameters derived from dual-layer spectral detector computed tomography for diagnosing metastatic cervical lymph nodes in patients with papillary thyroid cancer

Yan Zhou[1] · Yong-Kang Xu[1] · Di Geng[1] · Guo-Yi Su[1] · Xing-Biao Chen[2] · Yan Si[3] · Mei-Ping Shen[3] · Xiao-Quan Xu[1] · Fei-Yun Wu[1]

Abstract

Objective To investigate the added value of quantitative parameters derived from dual-layer spectral detector computed tomography (SDCT) for diagnosing metastatic cervical lymph nodes (LNs) in patients with papillary thyroid cancer (PTC).

Methods A total of 219 cervical LNs (121 non-metastatic and 98 metastatic) were enrolled from 73 patients with PTC. Conventional CT image features including enlarged size, abnormal enhancement, calcification, cystic change and extranodal extension were evaluated. SDCT-derived quantitative parameters including normalized iodine concentration (NIC), effective atomic number (Z_{eff-c}) and slope of energy spectrum curve (λ_{HU}) in both arterial phase and venous phase were measured and calculated. The $\chi 2$ or Fisher's precision probability test was used to compare qualitative CT image features. Mann–Whitney U test was used to compare quantitative parameters. Multivariate logistic regression analysis was applied to build three models based on conventional features (model 1), quantitative parameters (model 2) and their combination (model 3). ROC curves analysis was used to assess and compare the diagnostic performances.

Results Metastatic LNs demonstrated significantly higher NIC, Z_{eff-c}, and λ_{HU} in both arterial phase and venous phase than non-metastatic LNs (all $P < 0.001$). Model $1 = -1.477 + 1.902 \times$ abnormal enhancement $+ 2.414 \times$ calcification. Model $2 = -4.818 + 10.951 \times$ arterial phase NIC $+ 0.836 \times$ arterial phase λ_{HU}. Model $3 = -4.991 + 0.562 \times$ abnormal enhancement $+ 2.380 \times$ calcification $+ 10.624 \times$ arterial phase NIC $+ 0.779 \times$ arterial phase λ_{HU}. Model 3 showed the best performance (AUC $= 0.958$), followed by model 2 (AUC $= 0.954$). Both these two models overperformed model 1 (AUC $= 0.740$) (both $P < 0.001$).

Conclusion Compared with conventional CT image features alone, adding quantitative parameters derived from SDCT could improve the performance in diagnosing metastatic cervical LNs in patients with PTC.

Keywords Papillary thyroid cancer · Lymph node · Metastasis · Spectral computed tomography · Iodine concentration

Yan Zhou and Yong-Kang Xu have contributed equally to this work.

✉ Xiao-Quan Xu
xiaoquanxu_1987@163.com

✉ Fei-Yun Wu
wfy_njmu@163.com

1 Department of Radiology, The First Affiliated Hospital of Nanjing Medical University, No. 300, Guangzhou Rd, Gulou District, Nanjing, People's Republic of China

2 Section of Clinical Research, Philips Healthcare Ltd, Shanghai, China

3 Department of Thyroid Surgery, The First Affiliated Hospital of Nanjing Medical University, Nanjing, China

Abbreviations

LN	Lymph node
PTC	Papillary thyroid cancer
US	Ultrasonography
CT	Computed tomography
DECT	Dual-energy CT
SDCT	Spectral detector CT
SBI	Spectral base image
CTDIvol	CT dose index
DLP	Dose-length product
ROI	Region of interest
CCA	Common carotid artery
IC	Iodine concentration
NIC	Normalized iodine concentration
Z_{eff-c}	Effective atomic number

λ_{HU}	Slope of energy spectrum curve
HU	Hounsfield Unit
ICC	Intraclass correlation coefficient
VIF	Variance inflation factor
ROC	Receiver operating characteristic
PPV	Positive predictive value
NPV	Negative predictive value
CI	Confidence interval
IQR	Interquartile range

Introduction

Cervical lymph node (LN) metastasis is an important risk factor associated with the disease recurrence in patients with papillary thyroid cancer (PTC). Determination of the status of cervical LN metastasis is crucial for establishing the individual treatment plan [1–3]. Ultrasonography (US) is the first-line image technique to evaluate the metastatic LNs in PTC patients. However, US depends on the operator experience. By contrast, contrast-enhanced computed tomography (CT) can overcome this shortage [4–6]. In clinical practice, radiologists usually assess the cervical LN based on the qualitative image features; however, it is restricted by its subjectivity [4–6]. Besides that, the positive rate is not very high due to some small metastatic LNs from PTC. Typical image features (e.g., abnormal enhancement, calcification, cystic change, extranodal extension) are usually absent on CT images of the small metastatic LNs. Therefore, a more quantitative and accurate method is desirable.

Dual-energy CT (DECT) can obtain massive data under two energies, and subsequently classify different tissues based on the difference of photon absorption [7, 8]. It can provide specific quantitative parameters reflecting tissue characteristics after uncomplicated imaging post-processing [7–10]. DECT has been widely used in improving image quality, differentiating malignant from benign lesions, quantitatively identifying different substances (iodine, calcium, uric) [7–10]. Besides, DECT has been verified to be useful in diagnosing the metastatic LNs in different types of malignant tumors [10–12]. With regard to PTC, some previous studies have proven that DECT-derived quantitative metrics can help to differentiate metastatic from non-metastatic LNs [13–17]. Rapid kVp switching and dual-source CT were two commonly used DECT techniques for assessing the metastatic LNs from patients with PTC in previous studies [13–17].

Besides the above-mentioned two DECT techniques, dual-layer spectral detector computed tomography (SDCT) equipped with single X-ray tube and two spatially equivalent upper and lower layers attracts increasingly attention [18]. Compared with other DECT techniques, SDCT is more convenient for clinical use. It does not change the conventional work flow, and it has high time resolution [18]. SDCT can automatically generate the spectral base image (SBI) datasets integrated with an iterative reconstruction algorithm, which can be analyzed retrospectively with no need of further image processing [18–21]. Moreover, SDCT image data is analyzed in completely matched time and space, making it more simultaneous and homologous [18–22]. Besides that, SDCT applies the anti-correlation noise reduction technology, which can effectively reduce the spectral image noise and improve the quality [23]. To date, the study investigating the value of SDCT-derived quantitative parameters in diagnosing cervical metastatic LNs in patients with PTC is still lacked.

Therefore, this study aimed to explore the added value of quantitative parameters derived from SDCT to conventional CT image features, in the differential diagnosis of cervical metastatic LNs in patients with PTC.

Materials and methods

Patients selection

This retrospective study was approved by the ethic committee of our institutional review board, and written informed consent was waived due to the retrospective nature. A total of 186 patients with suspicious PTC who underwent pre-operative SDCT scan for pre-treatment evaluation between November 2021 to May 2022 were enrolled. The inclusion criteria were as follows: (1) PTC confirmed by postoperative pathology; (2) cervical LNs dissection was conducted and had pathological results; (3) no history of other cancers; and (4) image quality was adequate for subsequent analyses. Finally, 73 patients (18 men, 55 women; mean age, 43 years; age range, 24–77 years) with PTC were included in this study.

LNs histopathologic labeling and assignment

All cervical LNs were divided into 7 levels with reference to American Joint Committee on Cancer cervical regional lymph node level system [24]. The surgeons conducted the cervical LNs dissection, and sent the surgical specimens to the department of pathology level by level. Then, experienced pathologists would make a diagnosis of the LNs level by level. The assignment and grouping of cervical LNs were performed with reference to the method proposed in the study of Park JE et al. [6], for solving the problems of LNs matching between pathological and radiological results in retrospective study. The specific method was as follows: When all the surgically harvested LNs in one cervical level were pathologically reported to be negative, all the identified LNs on CT images in this level were regarded as

non-metastatic. When all the surgically harvested LNs in one cervical level were pathologically reported to be positive, all the identified LNs on CT images in this level were regarded as metastatic. When one cervical level comprised both non-metastatic and metastatic LNs pathologically confirmed, then all the LNs on CT images in this level were ruled out for further analyses [6, 16]. To avoid the potential risk of false "all positive" or "all negative" in one cervical level, if only one LN in one specific cervical level was surgically harvested and pathologically analyzed, then the LN would also be discarded. Only the LNs with a maximal diameter in short axial of > 5 mm were included in the study for avoiding the partial volume effect. Finally, a total of 219 cervical LNs (121 non-metastatic and 98 metastatic) were included in this study.

SDCT acquisition and post-processing

All patients underwent dual-phase contrast-enhanced SDCT examinations (IQon Dual-Layer spectral CT, Philips Healthcare). Acquisition parameters were detailed as follows: tube voltage, 120 kVp; tube current, modulated by automatic radiation exposure control; detector collimation, 64×0.625 mm; rotation time, 0.5 s; helical pitch, 1.1. All patients were injected with 75 mL of contrast medium (iopromide; Bayer HealthCare) in the right elbow vein at a the rate of 3.5 mL/sec, followed by a saline flash of 25 mL at the same rate. The scan delay times for the early arterial and venous phases were 25 s and 50 s, respectively. All original images were reconstructed as SBI datasets with a slice thickness of 1 mm. All SBI datasets were transmitted to post-processing workstation (IntelliSpace Protal, Version 10, Philips Healthcare). The 120-kVp equivalent blended images were reconstructed by an iterative algorithm (iDose[4] [level 3], Philips Healthcare), while iodine maps were reconstructed by a Dual-Layer spectral reconstruction algorithm (Dual-Layer spectral [level 3], Philips Healthcare) [21, 22].

CT dose index (CTDIvol) and dose-length product (DLP) were recorded to evaluate the radiation dose. The total mean volume CTDIvol and DLP was 14.3 ± 2.9 mGy (range, 10.9–20.1 mGy) and 394.7 ± 72.5 mGy $\times$ cm (range, 303.9–559.9 mGy $\times$ cm), respectively.

Qualitative CT image features

Two radiologists (with 6 and 5 years of experience in head and neck radiology, respectively) who were blinded to the clinicopathologic results and study design, evaluated the morphological CT image features based on the 120-kVp equivalent blended CT images. If disagreements existed, the third senior radiologist (with 26-year experience in head and neck imaging) would make the consensus.

CT-reported positive image features for metastatic LNs were listed as follows: (1) a maximal diameter in short axis of ≥ 10 mm; (2) abnormal enhancement referred to strong or heterogeneous enhancement; (3) calcification; (4) cystic change; (5) extranodal extension referred to fuzzy boundary or invasion into surrounding structures [6, 13]. If one of these positive CT image features was present, the LN was reported as positive, otherwise the LN was reported as negative.

Quantitative SDCT-derived parameters

Manual regions of interest (ROIs) were drawn comprising the whole LNs. During the placement of ROIs, calcification and cystic area were excluded. Meanwhile, another ROI was drawn (about 15 ± 5 mm^2) on the ipsilateral common carotid artery (CCA) for iodine concentration (IC) normalization. IC was measured on arterial and venous phases iodine maps. Effective atomic number (Z_{eff-c}) was measured on arterial and venous phases Z_{eff-c} maps. Spectral curves were generated and Hounsfield Units (HUs) were measured on arterial and venous phases 40 keV and 70 keV images. Normalized iodine concentration (NIC) was calculated using the following equation: $NIC = IC_{LN}/IC_{CCA}$. IC_{LN} and IC_{CCA} were the IC of LNs and CCA, respectively. Slope of energy spectrum curve (λ_{HU}) was calculated using the following equation: $\lambda_{HU} = (HU_{40kev}-HU_{70kev})/(70kev-40kev)$. HU_{40kev} and HU_{70kev} were the HUs measured on 40 keV and 70 keV images, respectively [13] (Fig. 1). After measurement and calculation, six quantitative parameters (arterial and venous phase NIC, Z_{eff-c} and λ_{HU}) were derived from SDCT for each LN.

Quantitative measurements were also performed by above-mentioned two radiologists. Average values of these two radiologists were taken for final analyses.

Statistical analyses

Statistical analyses were performed using SPSS (version 23.0, SPSS, Chicago, IL, USA) and MedCalc (version 15.0, MedClac, Mariakerke, Belgium) software. Interobserver agreement of qualitative image features between two radiologists was evaluated using Cohen's kappa statistic. The agreement was interpreted as perfect (kappa > 0.80), fair (kappa = 0.60–0.80), moderate (kappa = 0.40–0.60), or poor (kappa < 0.40) [25]. The consistency of SDCT-derived quantitative parameters between two radiologists was assessed using intraclass correlation coefficient (ICC). The agreement was defined as perfect (ICC > 0.90), fair (ICC = 0.75–0.90), moderate (ICC = 0.50–0.75), or poor (ICC < 0.50) [26]. The normality of data was evaluated by using Kolmogorov–Smirnov test. Normally distributed variables were expressed as mean $\pm$ standard deviation, and t-test
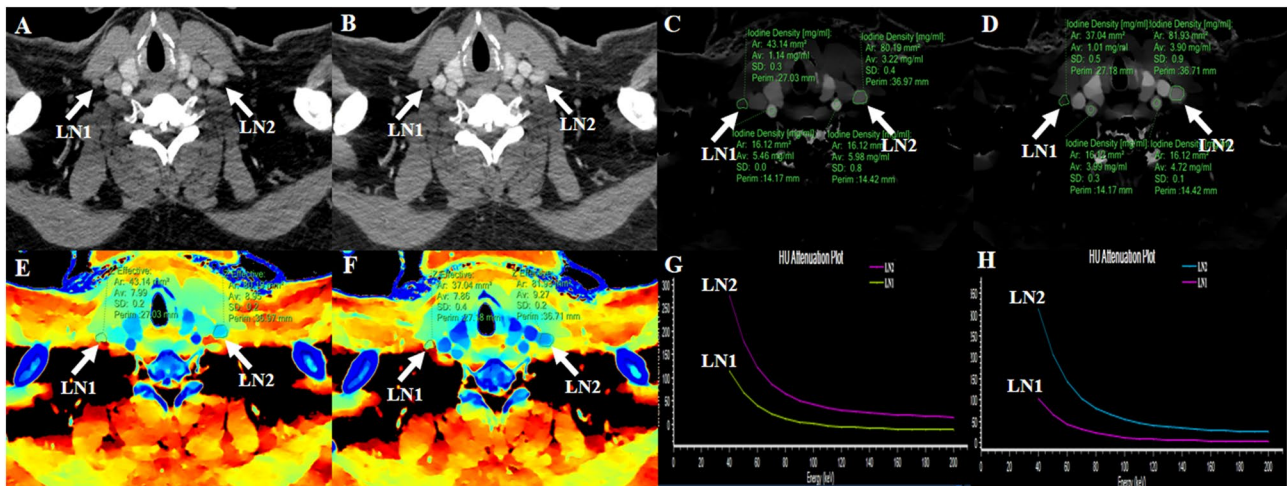
Fig. 1 SDCT images of a 32-year-old male patient with bilateral PTC. A non-metastatic LN1 was identified in the right III level, and another metastatic LN2 was found in the left III level. LN2 showed more obvious enhancement than LN1 in both arterial and venous 120-kVp equivalent blended images (**A**, **B**). ROIs were manually drawn on arterial and venous phase iodine map (**C**, **D**) and Z_{eff-c} maps (**E**, **F**), respectively. Meanwhile, some other circle ROIs were manually drawn on ipsilateral CCA for normalization. Spectral curves were generated, and λ_{HU} was calculated in both arterial and venous phase (**G**, **H**), respectively. Arterial phase NIC, Z_{eff-c} and λ_{HU} of LN1 vs LN2 was 0.21 vs 0.54, 7.99 vs 8.95, 3.08 vs 6.50, respectively. Venous phase NIC, Z_{eff-c} and λ_{HU} of LN1 vs LN2 was 0.25 vs 0.83, 7.86 vs 9.27, 2.50 vs 6.67, respectively

was used to compare the differences. Otherwise, variables were expressed as median (range), and Mann–Whitney U test was used. The $\chi2$ test or Fisher's precision probability test was applied to compare the qualitative LNs features between two groups. Variables with P values < 0.05 were put into the multivariate logistic regression analyses using stepwise method to build three models based on conventional CT image features (model 1), quantitative parameters (model 2) and their combination (model 3), respectively [27]. Calculation formulae were generated for three models. Variance inflation factor (VIF) was checked for each variable to avoid multicollinearity [28]. Diagnostic performances were assessed using receiver operating characteristic (ROC) curves analyses, and compared using Delong method [29]. A two-sided P value < 0.05 was considered to be statistically significant.

Results

LNs labeling and grouping

Two hundred and nineteen cervical LNs (121 non-metastatic and 98 metastatic) from 73 patients with PTC were finally included in the study. The location of 121 enrolled non-metastatic LNs was as follows: (1) II level with 41 LNs (33.9%); (2) III level with 14 LNs (11.6%); (3) IV level with 30 LNs (24.8%); (4) V level with 11 LNs (9.1%); and (5) VI level with 25 LNs (20.7%). The location of included 98 metastatic LNs was as follows: (1) II level with 9 LNs (9.2%);

(2) III level with 13 LNs (13.3%); (3) IV level with 28 LNs (28.6%); (4) V level with 2 LNs (2.0%); and (5) VI level with 46 LNs (46.9%).

Conventional CT image features

The agreements between two radiologists for all qualitative image features were perfect (all kappa > 0.80). CT-reported positive LNs was 67.3% (66 of 98) in metastatic cervical LNs. The incidence rate of size > 10 mm, abnormal enhancement, calcification, cystic change and extranodal extension in metastatic LNs group was 24.5%, 59.2%, 13.3%, 10.2% and 2.0%, respectively. CT-reported negative LNs was 79.3% (96 of 121) in non-metastatic cervical LNs. Conventional morphological features for diagnosing metastatic cervical LNs are detailed in Table 1.

Quantitative SDCT-derived parameters

The consistencies between two radiologists for all quantitative parameters were fair (all ICCs > 0.75). All quantitative parameters in metastatic LNs group were significantly higher than those in non-metastatic LNs group for total LNs, CT-reported positive and negative LNs ($P < 0.001$). Detailed comparisons of quantitative parameters derived from SDCT between two groups are summarized in Table 2. The diagnostic performances of these quantitative parameters were favorable (all AUCs > 0.800). Among them, arterial phase NIC yielded the highest diagnostic ability with an AUC of 0.944, a sensitivity of 0.918, a specificity of 0.826, a positive

Table 1 Comparison of conventional CT image features between non-metastatic and metastatic LNs

Features	Non-meta-static LNs (121)	Metastatic LNs (98)	P value
CT-reported positive signs	25 (20.7%)	66 (67.3%)	
Size (mm)	6.7 ± 1.7	11.2 ± 2.6	0.001[a]
Size > 10 mm	15 (12.4%)	24 (24.5%)	0.020[b]
Abnormal enhance-ment	20 (16.5%)	58 (59.2%)	< 0.001[b]
Calcification	0 (0.0%)	13 (13.3%)	< 0.001[c]
Cystic change	0 (0.0%)	10 (10.2%)	< 0.001[c]
Extranodal extension	0 (0.0%)	2 (2.0%)	0.199[c]

Size is expressed as mean ± standard deviation. Other data are numbers of lymph nodes and parentheses indicate the proportion

LNs lymph nodes

[a]Calculated using *t*-test

[b]Calculated using $\chi 2$ test

[c]Calculated using Fisher's precision probability test

predictive value (PPV) of 0.811 and a negative predictive value (NPV) of 0.926.

For CT-reported LNs-negative group, these parameters also demonstrated good diagnostic efficiencies (all AUCs > 0.700). Arterial phase NIC also possessed the highest diagnostic performance with an AUC of 0.788, a sensitivity of 0.719, a specificity of 0.722, a PPV of 0.635 and a NPV of 0.852. Detailed discriminative abilities of these parameters for diagnosing the metastatic LNs in both total LNs group and CT-reported LNs-negative group are summarized in Table 3 and depicted in Fig. 2.

Multivariate logistic regression analyses

Statistically significant variables were put into multivariate logistic regression analyses, and three models were built based on conventional CT image features (model 1), quantitative parameters (model 2) and their combination (model 3). Calculation formula for model $1 = -1.477 + 1.902 \times$ abnormal enhancement $+ 2.414 \times$ calcification. Calculation formula for model $2 = -4.818 + 10.951 \times$ arterial phase NIC $+ 0.836 \times$ arterial phase λ_{HU}. Calculation formula for model $3 = -4.991 + 0.562 \times$ abnormal enhancement $+ 2.380 \times$ calcification $+ 10.624 \times$ arterial phase

Table 2 Comparison of SDCT-derived parameters between non-metastatic and metastatic LNs

Parameters	Non-metastatic LNs (121)	Metastatic LNs (98)	P value
Total LNs			
Arterial phase NIC	0.10 (0.06–0.14)	0.38 (0.28–0.50)	< 0.001[a]
Arterial phase Z_{eff-c}	7.71 (7.54–8.25)	9.24 (8.50–12.59)	< 0.001[a]
Arterial phase λ_{HU}	1.51 (1.08–1.99)	4.99 (3.07–6.37)	< 0.001[a]
Venous phase NIC	0.28 (0.21–0.36)	0.66 (0.44–0.82)	< 0.001[a]
Venous phase Z_{eff-c}	8.05 (7.90–8.49)	9.27 (8.58–14.23)	< 0.001[a]
Venous phase λ_{HU}	2.51 (2.03–3.14)	4.98 (3.52–5.94)	< 0.001[a]
CT-reported positive LNs			
Arterial phase NIC	0.10 (0.08–0.14)	0.40 (0.29–0.50)	< 0.001[a]
Arterial phase Z_{eff-c}	7.75 (7.60–8.12)	9.50 (8.57–13.6)	< 0.001[a]
Arterial phase λ_{HU}	1.64 (1.19–2.26)	5.05 (3.63–6.49)	< 0.001[a]
Venous phase NIC	0.34 (0.23–0.44)	0.70 (0.63–0.89)	< 0.001[a]
Venous phase Z_{eff-c}	8.10 (7.97–8.47)	9.49 (8.61–14.23)	< 0.001 [a]
Venous phase λ_{HU}	2.71 (2.25–3.62)	4.98 (4.12–5.97)	< 0.001[a]
CT-reported negative LNs			
Arterial phase NIC	0.14 (0.10–0.22)	0.26 (0.16–0.37)	< 0.001[a]
Arterial phase Z_{eff-c}	7.70 (7.47–9.20)	8.82 (7.98–11.84)	< 0.001[a]
Arterial phase λ_{HU}	1.59 (1.25–1.96)	3.43 (2.95–4.09)	< 0.001[a]
Venous phase NIC	0.26 (0.20–0.33)	0.44 (0.29–0.65)	< 0.001[a]
Venous phase Z_{eff-c}	8.02 (7.81–9.73)	9.14 (8.38–13.48)	< 0.001 [a]
Venous phase λ_{HU}	2.37 (1.78–2.89)	3.34 (2.49–4.65)	< 0.001[a]

SDCT-derived parameters are expressed as median with interquartile range in parentheses

LNs lymph nodes, *NIC* normalized iodine concentration, Z_{eff-c} effective atomic number, λ_{HU} slope of energy spectrum curve

[a]Calculated using Mann–Whitney *U* test

Table 3 Diagnostic performances of SDCT-derived parameters for diagnosing metastatic LNs

	AUC	Sensitivity	Specificity	PPV	NPV
Total LNs					
Arterial phase NIC	0.944 (0.904, 0.970)	0.918 (0.845, 0.964)	0.826 (0.747, 0.889)	0.811 (0.725, 0.879)	0.926 (0.859, 0.967)
Arterial phase Z_{eff-c}	0.844 (0.790, 0.890)	0.939 (0.871, 0.977)	0.703 (0.613, 0.782)	0.719 (0.632, 0.795)	0.934 (0.862, 0.975)
Arterial phase λ_{HU}	0.939 (0.899, 0.967)	0.888 (0.808, 0.943)	0.860 (0.785, 0.916)	0.837 (0.751, 0.902)	0.904 (0.835, 0.951)
Venous phase NIC	0.851 (0.796, 0.895)	0.755 (0.658, 0.836)	0.884 (0.813, 0.935)	0.841 (0.748, 0.910)	0.817 (0.740, 0.879)
Venous phase Z_{eff-c}	0.832 (0.776, 0.879)	0.918 (0.845, 0.964)	0.694 (0.604, 0.775)	0.709 (0.621, 0.786)	0.913 (0.836, 0.962)
Venous phase λ_{HU}	0.859 (0.806, 0.902)	0.765 (0.669, 0.845)	0.835 (0.756, 0.896)	0.789 (0.694, 0.866)	0.815 (0.735, 0.879)
CT-reported negative LNs					
Arterial phase NIC	0.788 (0.697, 0.862)	0.719 (0.533, 0.863)	0.722 (0.604, 0.821)	0.635 (0.477, 0.788)	0.852 (0.738, 0.930)
Arterial phase Z_{eff-c}	0.757 (0.663, 0.836)	0.838 (0.692, 0.892)	0.697 (0.575, 0.811)	0.608 (0.475, 0.741)	0.856 (0.749, 0.895)
Arterial phase λ_{HU}	0.766 (0.673, 0.844)	0.750 (0.566, 0.885)	0.792 (0.680, 0.878)	0.615 (0.446, 0.766)	0.877 (0.772, 0.945)
Venous phase NIC	0.723 (0.626, 0.806)	0.713 (0.536, 0.828)	0.711 (0.589, 0.824)	0.681 (0.543, 0.822)	0.780 (0.657, 0.855)
Venous phase Z_{eff-c}	0.770 (0.678, 0.847)	0.775 (0.671, 0.865)	0.722 (0.604, 0.821)	0.683 (0.532, 0.824)	0.829 (0.727, 0.880)
Venous phase λ_{HU}	0.729 (0.632, 0.811)	0.657 (0.468, 0.814)	0.819 (0.711, 0.900)	0.618 (0.436, 0.778)	0.843 (0.736, 0.919)

Data in parentheses indicate 95% confidence interval

LNs lymph nodes, *NIC* normalized iodine concentration, Z_{eff-c} effective atomic number, λ_{HU} slope of energy spectrum curve, *PPV* positive predictive value, *NPV* negative predictive value
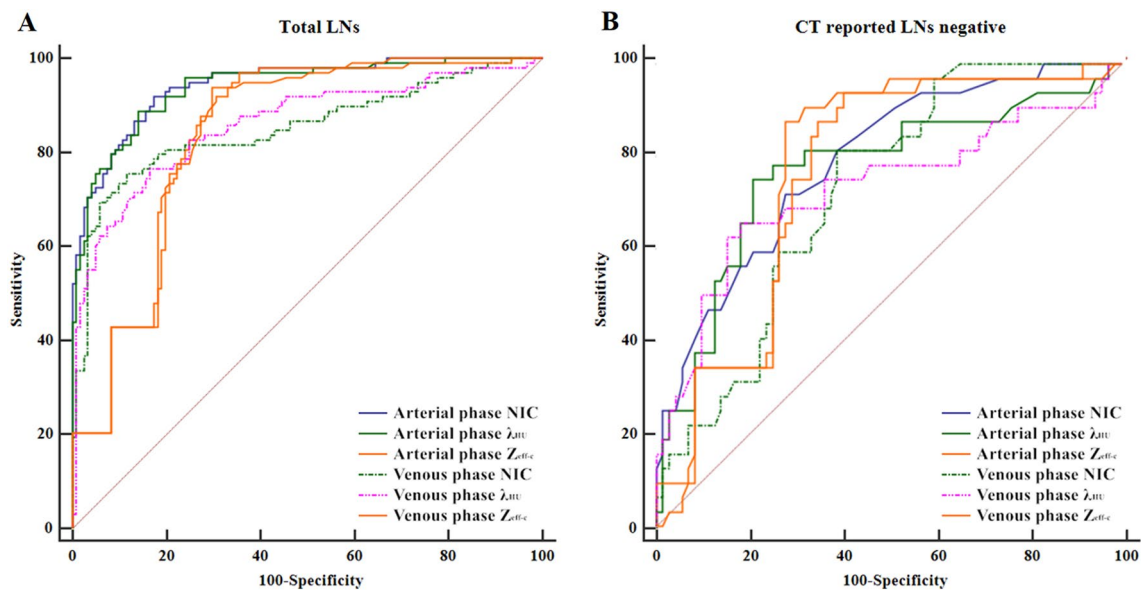

Fig. 2 ROC curve analysis of SDCT-derived parameters for diagnosing the metastatic LNs in both total LNs (**A**) and CT-reported negative LNs group (**B**)

NIC + 0.779 × arterial phase λ_{HU}. Results of multivariate logistic regression analyses are summarized in Table 4.

Added value of quantitative parameters

Model 3 demonstrated the optimal diagnostic performance with an AUC of 0.958, a sensitivity of 0.908, a specificity of 0.893, a PPV of 0.873 and a NPV of 0.923.

The performance was followed by model 2 with an AUC of 0.954, a sensitivity of 0.888, a specificity of 0.908, a PPV of 0.879 and a NPV of 0.908. Both these two models overperformed model 1 (AUC = 0.740; both *P* < 0.001). Diagnostic performances of conventional features, quantitative parameters and their combination are detailed in Table 5, and ROC curves are shown in Fig. 3.

Table 4 Results of multivariate logistic regression analyses

Variable	Coefficient	SD	Odds (95% CI)	P value	VIF
Conventional features					
Abnormal enhancement	1.902	0.327	6.700 (3.533, 12.707)	< 0.001	1.037
Calcification	2.414	1.077	11.179 (1.353, 92.372)	0.025	1.037
Quantitative parameters					
Arterial phase NIC	10.951	2.637	5.7×10^4 (3.2×10^2, 1.0×10^7)	< 0.001	3.165
Arterial phase λ_{HU}	0.836	0.237	2.308 (1.451, 3.671)	< 0.001	3.165
Combination					
Abnormal enhancement	0.562	0.499	1.755 (0.660, 4.663)	0.017	1.340
Calcification	2.380	1.749	10.807 (0.351, 333.084)	0.026	1.080
Arterial phase NIC	10.624	2.701	4.1×10^4 (2.1×10^2, 8.2×10^6)	< 0.001	3.257
Arterial phase λ_{HU}	0.779	0.249	2.179 (1.339, 3.548)	0.002	3.330

Data in parentheses indicate 95% confidence interval

NIC normalized iodine concentration, λ_{HU} slope of energy spectrum curve, *SD* standard deviation, *CI* confidence interval, *VIF* variance inflation factor

Table 5 Added value of quantitative parameters to conventional features for diagnosing metastatic LNs

Indicator	Conventional features	Quantitative parameters	Combination
AUC	0.740 (0.677, 0.797)	0.954 (0.918, 0.978)	0.958 (0.923, 0.981)
Sensitivity	0.816 (0.725, 0.887)	0.888 (0.808, 0.943)	0.908 (0.833, 0.957)
Specificity	0.620 (0.527, 0.707)	0.908 (0.833, 0.948)	0.893 (0.823, 0.942)
PPV	0.635 (0.544, 0.719)	0.879 (0.798, 0.936)	0.873 (0.792, 0.930)
NPV	0.806 (0.711, 0.881)	0.908 (0.842, 0.953)	0.923 (0.859, 0.964)

Data in parentheses indicate 95% confidence interval

LNs lymph nodes, *PPV* positive predictive value, *NPV* negative predictive value
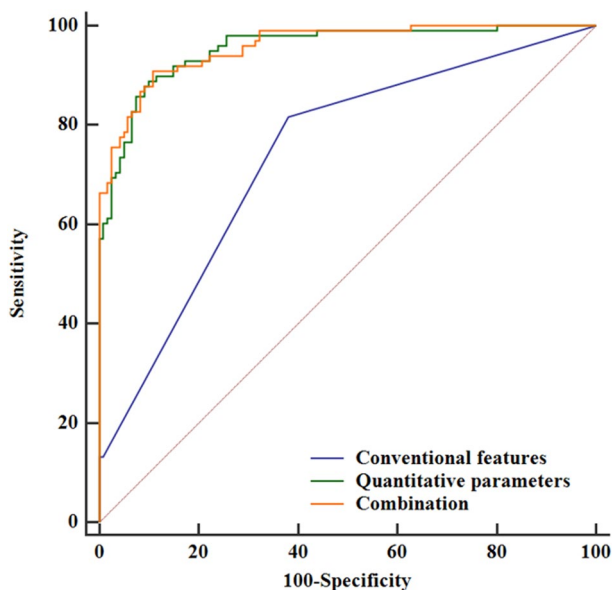
Fig. 3 Diagnostic performances of conventional features, quantitative parameters and their combination

Discussion

In this study, we found that all quantitative parameters derived from SDCT of metastatic LNs were significantly higher than those of non-metastatic LNs. All these quantitative parameters performed well in diagnosing LNs metastasis from PTC, even in the CT-reported LNs-negative group. And we found that the model adding quantitative parameters derived from SDCT to conventional CT image features could further improve the performance in diagnosing metastatic cervical LNs in patients with PTC.

In clinical practice, conventional CT image features, such as enlarged size, abnormal enhancement, calcification, cystic change and extranodal extension, were widely used in diagnosing the metastatic cervical LNs from PTC [5, 6, 13]. However, it was limited for the subjectivity. Moreover, the detection rate of these positive CT image signs was usually unsatisfactory due to the lack of typical image features in small-sized LNs [1, 4, 5]. In our study, the incidence of size > 10 mm, calcification, cystic change and extranodal extension was relatively low (all < 25%) in metastatic LNs group. And the diagnostic value was also limited for model 1 based on these CT image features in

our study. This diagnostic dilemma would affect the establishment of surgical plan to a certain extent. Therefore, a more quantitative and accurate method was needed in clinical practice.

In our study, NIC, Z_{eff-c}, and λ_{HU} of metastatic LNs were significantly higher than those of non-metastatic LNs in both arterial and venous phase, which was in consistent with previous studies [13–15]. Increased blood supply and abnormal vascularity was found in metastatic LNs in previous researches [31, 32]. The increased blood supply might cause the increased iodine concentration, which may subsequently bring about the increased NIC, Z_{eff-c} and λ_{HU} [13–15]. It was worth discussing that arterial phase NIC performed best among all these parameters. This finding was consistent with previous studies, which found that obvious enhancement in early arterial phase was a significant image characteristic of metastatic LNs in PTC patients [6, 33]. In addition, our study found that these parameters could also achieve satisfactory diagnostic performances, even in the CT-reported LNs-negative group. These results suggested that quantitative parameters derived from SDCT could detect earlier changes of internal structure in metastatic LNs than conventional CT image features.

We built three models for conventional CT image features alone (model 1), quantitative parameters alone (model 2) and their combination (model 3), respectively. We found that model 3 performed the best, followed by model 2. Both these two models significantly outperformed model 1. These results indicated that SDCT-derived quantitative parameters could be an important supplement to conventional CT image features for diagnosing cervical LNs metastasis, and SDCT scan model was suggested to be used for assessing the metastatic cervical LNs in patients with PTC in clinical practice.

Compared with the other DECT techniques (rapid kVp switching, dual-source CT), SDCT generated X-ray spectrum based on dual-layer detector. Low-energy photons were absorbed by the upper layer, while high-energy photons were absorbed by the lower layer, which allowed the energy data transmitted from the corresponding side data channels [18]. SDCT working principle permitted it to generate more simultaneous and homologous image data [18–22]. Besides that, SDCT used the anti-correlation noise reduction technology, which could effectively reduce the spectral image noise and improve the quality [23]. Considering these technological advantages, SDCT and its derived quantitative metrics might be promising in diagnosing the metastatic cervical LNs in patients with PTC.

There were several limitations that should be noted in this study. First, the sample size was relatively small. Future study with larger sample size would be needed to verify the results. Second, due to the retrospective nature, we could not correspond the radiological LNs to the pathological LNs one by one. Third, dual-phase contrast-enhanced CT scan

might lead to the increase of the radiation dose to a certain degree. Effective techniques would be needed to reduce the radiation exposure.

In conclusion, SDCT and its derived quantitative parameters are effective in diagnosing the metastatic cervical LNs in patients with PTC, even in the CT-reported LNs-negative group. Adding SDCT-derived qualitative parameters to conventional image features can furthermore improve the diagnostic performance.

Data availability The datasets used and analyzed for this study are available on request to the corresponding authors.

Declarations

Conflict of interest The authors certify that there is no actual or potential conflict of interest related to this study. On behalf of all authors, the corresponding authors state that there is no conflict of interest.

Ethics approval and consent to participate This study was approved by the Ethic Committee of The First Affiliated Hospital of Nanjing Medical University, and written informed consent was waived due to the nature of retrospective study.

References

1. Haugen BR, Alexander EK, Bible KC, Doherty GM, Mandel SJ, Nikiforov YE, et al. 2015 American thyroid association management guidelines for adult patients with thyroid nodules and differentiated thyroid cancer: the american thyroid association guidelines task force on thyroid nodules and differentiated thyroid cancer. Thyroid. 2016;26(1):1–133.
2. Shirley LA, Jones NB, Phay JE. The role of central neck lymph node dissection in the management of papillary thyroid cancer. Front Oncol. 2017;7:122.
3. Zhang J, Cheng X, Shen L, Wang X, Wang L, Sun X, et al. The association between lymph node stage and clinical prognosis in thyroid cancer. Front Endocrinol (Lausanne). 2020;27(11):90.
4. Yang J, Zhang F, Qiao Y. Diagnostic accuracy of ultrasound, CT and their combination in detecting cervical lymph node metastasis in patients with papillary thyroid cancer: a systematic review and meta-analysis. BMJ Open. 2022;12(7): e051568.
5. Cho SJ, Suh CH, Baek JH, Chung SR, Choi YJ, Lee JH. Diagnostic performance of CT in detection of metastatic cervical lymph

nodes in patients with thyroid cancer: a systematic review and meta-analysis. Eur Radiol. 2019;29(9):4635–47.

6. Park JE, Lee JH, Ryu KH, Park HS, Chung MS, Kim HW, et al. Improved diagnostic accuracy using arterial phase ct for lateral cervical lymph node metastasis from papillary thyroid cancer. AJNR Am J Neuroradiol. 2017;38(4):782–8.

7. McCollough CH, Leng S, Yu L, Fletcher JG. Dual- and multi-energy CT: principles, technical approaches, and clinical applications. Radiology. 2015;276(3):637–53.

8. Patino M, Prochowski A, Agrawal MD, Simeone FJ, Gupta R, Hahn PF, et al. Material separation using dual-energy CT: current and emerging applications. Radiographics. 2016;36(4):1087–105.

9. Rajiah P, Parakh A, Kay F, Baruah D, Kambadakone AR, Leng S. Update on multienergy CT: physics, principles, and applications. Radiographics. 2020;40(5):1284–308.

10. Agrawal MD, Pinho DF, Kulkarni NM, Hahn PF, Guimaraes AR, Sahani DV. Oncologic applications of dual-energy CT in the abdomen. Radiographics. 2014;34(3):589–612.

11. Qiu L, Hu J, Weng Z, Liu S, Jiang G, Cai X. A prospective study of dual-energy computed tomography for differentiating metastatic and non-metastatic lymph nodes of colorectal cancer. Quant Imaging Med Surg. 2021;11(8):3448–59.

12. Martin SS, Czwikla R, Wichmann JL, Albrecht MH, Lenga L, Savage RH, et al. Dual-energy CT-based iodine quantification to differentiate abdominal malignant lymphoma from lymph node metastasis. Eur J Radiol. 2018;105:255–60.

13. Liu X, Ouyang D, Li H, Zhang R, Lv Y, Yang A, et al. Papillary thyroid cancer: dual-energy spectral CT quantitative parameters for preoperative diagnosis of metastasis to the cervical lymph nodes. Radiology. 2015;275(1):167–76.

14. Zhao Y, Li X, Li L, Wang X, Lin M, Zhao X, et al. Preliminary study on the diagnostic value of single-source dual-energy CT in diagnosing cervical lymph node metastasis of thyroid carcinoma. J Thorac Dis. 2017;9(11):4758–66.

15. He M, Lin C, Yin L, Lin Y, Zhang S, Ma M. Value of dual-energy computed tomography for diagnosing cervical lymph node metastasis in patients with papillary thyroid cancer. J Comput Assist Tomogr. 2019;43(6):970–5.

16. Zhou Y, Su GY, Hu H, Ge YQ, Si Y, Shen MP, et al. Radiomics analysis of Dual-Layer spectral detector CT-derived iodine maps for diagnosing metastatic cervical lymph nodes in patients with papillary thyroid cancer. Eur Radiol. 2020;30(11):6251–62.

17. Zou Y, Zheng M, Qi Z, Guo Y, Ji X, Huang L, et al. Dual-energy computed tomography could reliably differentiate metastatic from non-metastatic lymph nodes of less than 0.5 cm in patients with papillary thyroid carcinoma. Quant Imaging Med Surg. 2021;11(4):1354–1367.

18. Rassouli N, Etesami M, Dhanantwari A, Rajiah P. Detector-based spectral CT with a novel dual-layer technology: principles and applications. Insights Imaging. 2017;8(6):589–98.

19. Chae EJ, Song JW, Seo JB, Krauss B, Jang YM, Song KS. Clinical utility of Dual-Layer spectral detector CT in the evaluation of solitary pulmonary nodules: initial experience. Radiology. 2008;249(2):671–81.

20. den Harder AM, Bangert F, van Hamersvelt RW, Leiner T, Milles J, Schilham AMR, et al. The effects of iodine attenuation on pulmonary nodule volumetry using novel dual-layer computed tomography reconstructions. Eur Radiol. 2017;27(12):5244–51.

21. Lu X, Lu Z, Yin J, Gao Y, Chen X, Guo Q. Effects of radiation dose levels and spectral iterative reconstruction levels on the accuracy of iodine quantification and virtual monochromatic CT numbers in dual-layer spectral detector CT: an iodine phantom study. Quant Imaging Med Surg. 2019;9(2):188–200.

22. Gao L, Lu X, Wen Q, Hou Y. Added value of spectral parameters for the assessment of lymph node metastasis of lung cancer with dual-layer spectral detector computed tomography. Quant Imaging Med Surg. 2021;11(6):2622–33.

23. Primak AN, Giraldo JC, Eusemann CD, Schmidt B, Kantor B, Fletcher JG, et al. Dual-source Dual-Layer spectral detector CT with additional tin filtration: Dose and image quality evaluation in phantoms and in vivo. AJR Am J Roentgenol. 2010;195(5):1164–74.

24. Robbins KT, Clayman G, Levine PA, Medina J, Sessions R, Shaha A, et al. Neck dissection classification update: revisions proposed by the American head and neck society and the American academy of otolaryngology-head and neck surgery. Arch Otolaryngol Head Neck Surg. 2002;128(7):751–8.

25. Viera AJ, Garrett JM. Understanding interobserver agreement: the kappa statistic. Fam Med. 2005;37(5):360–3.

26. Koo TK, Li MY. A guideline of selecting and reporting intraclass correlation coefficients for reliability research. J Chiropr Med. 2016;15(2):155–63.

27. Zhang Z. Variable selection with stepwise and best subset approaches. Ann Transl Med. 2016;4(7):136.

28. O'brien RM. A caution regarding rules of thumb for variance inflation factors. Qual Quant. 2007;41(5):673–690.

29. Mandrekar JN. Receiver operating characteristic curve in diagnostic test assessment. J Thorac Oncol. 2010;5(9):1315–6.

30. Willard-Mack CL. Normal structure, function, and histology of lymph nodes. Toxicol Pathol. 2006;34(5):409–24.

31. Nathanson SD. Insights into the mechanisms of lymph node metastasis. Cancer. 2003;98(2):413–23.

32. Ji RC. Lymphatic endothelial cells, tumor lymphangiogenesis and metastasis: New insights into intratumoral and peritumoral lymphatics. Cancer Metastasis Rev. 2006;25(4):677–94.

33. Su GY, Xu XQ, Zhou Y, Zhang H, Si Y, Shen MP, et al. Texture analysis of dual-phase contrast-enhanced CT in the diagnosis of cervical lymph node metastasis in patients with papillary thyroid cancer. Acta Radiol. 2021;62(7):890–6.